PERIODICA POLYTECHNICA SER. TRANSP. ENG. VOL. 28, NO. 1–2, PP. 77–90 (2000)

NUMERICAL MODELLING OF THE MECHANICAL PROCESS OF PARTICLE DETACHMENT BY FINITE ELEMENT METHOD

András ELEŐD*, János DEVECZ* and Tibor BALOGH**

*Department of Vehicle Parts and Drives
Budapest University of Technology and Economics
H–1521 Budapest, Hungary
**Széchenyi István College
H–9026 Győr, Hungary

Received: Oct.10, 2000

Abstract

This paper presents a numerical simulation technique for calculating the strain and the stress state at every point of the surfaces, containing real surface topology and layered structure. Depending on the nature of deformation, we can evaluate the actual stress and strain state either from the point of view of the fatigue failure or from the point of view of the exhaustion of deformation capacity of the surfaces. Using the stress and strain components calculated by the Finite Element Method at every nodal point of the surfaces, it is possible to predict the probable surfaces degradation mechanism, i.e. to predict the probable mechanism of the particle detachment under dry sliding conditions, under consideration of the nominal load and to the required lifetime of the surface.

Keywords: tribology, numerical simulation, finite element method.

1. Introduction

Several researchers have been dealing with the possible forms, mechanisms and quantitative determination of wear developing from friction since the beginning of the century. These theories have a common feature, they do not differentiate between the mechanisms of initial wear and permanent wear and neither of them have satisfactory explanation for friction without wear.

In the recent decade, the ‘third body’ theory, the investigation and explanation of friction from a new viewpoint has come forward. Based on the results of the tests that are given by modern test machines, the ‘third body’ theory queries the usability and validity of the classical wear theories or wear mechanisms in some aspects. The ‘third body’ theory says that the friction mechanisms known so far explain only initial wear and not wear in the permanent stage of friction [1]. In the permanent stage of friction the particle detachment means the so-called inside source of the development of the ‘third body’ and only particles leaving the tribological system permanently are regarded as wear [2]. The wear is a result of a complex process, but the stipulation of the wear beginning is, in any case, the beginning of the particle detachment.

2. Possible Forms and Conditions of Particle Detachment of Metals

Particle detachment is the result of fracture occurring when the deformation capacity of the material is exhausted. Except for the extreme case of micro-cutting, the particle detachment can happen practically in three different ways:

- *in form of brittle fracture*: as a result of elastic stress state, without starting the plastic deformation, in consequence of a specific fracture work that is reduced to zero under influences of state-factors. In the case of centred metals of cubic lattice with the most sliding planes, fracture without plastic deformation is not expected to start. In the case of space centred metals of cubic lattice and even more in the case of metals of hexagonal lattice having one sliding plane, brittle fracture may occur following the joint effect of state factors. The particles approaching the brittle state at the moment friction begins and with their specific fracture work becoming zero, will fracture without plastic deformation. The detachment of these particles means the so-called initial wear experienced at the beginning of friction.
- *in form of fatigue fracture*: as a consequence of the cumulative damage, under elastic contact conditions. In the case of stress smaller than the yield point, taking the accumulation of damages into account, fracture occurs when the aggregate of the work of the elementary plastic deformations reaches all of the work necessary for fracture.
- *in form of ductile fracture*: when the strain of the given particle during deformation exceeds the critical limit values, i.e. the deformation capacity characteristic of the material of given state.

From the possible procedures that are traceable to mechanical causes of the particle detachment, it is possible to indicate in advance the development of the fatigue fracture and the ductile fracture. By the help of the Finite Element Method, we can determine at every nodal point of the model the components of the stress and strain states, in function of the external load and of the geometry of sliding surfaces.

In the following sections, we would like to show, with the help of FEM-simulations of dry friction, how we could predict the expected form of the surface degradation for a given surface topology and material properties.

3. Real Surface Contact Model

The numerical modelling of contact problems – due to the development of the computing technology – suffered a significant change during the last years. From the linear-elastic 2D solution to the non-linear 3D elastic-plastic solution every step of the development can be followed in the literature. However, the latest studies in this field are restricted either to the two-dimensional analytical solution of the elastic-plastic problem [3], [4], [5] or to the approximate solution of the 3D

contact [6], [7], [8], [9]. Authors using the approximate three- dimensional solutions assume frequently elastic perfectly-plastic material behaviour and/or axisymmetric coordinate system.

Our numerical simulation is based on the solutions by Finite Element Method of the three-dimensional contact of surfaces which is characterised by non-linear hardening law and by real topography. FEM is preferred for the contact simulation, because it can place in our disposal all components of the strain and stress states at every moment of the movement and at every grid point on the surfaces.

To simulate 3D contact, first it is necessary to develop the geometrical model of the surfaces. For developing rough surfaces, there are basically two options:

- to generate a surface roughness with the help of individual roughness contours [10], [11] [6], [12] or with specified auto-correlation function and distribution function of roughness peaks [13], [14], [15],
- to use the measured surface topography in discretized form [7], [9], or in digitalized form.

In the second case, the discretization signifies the connecting of the measured roughness values by line sections in both directions, so the surface will be covered by elementary squares. The digitalization of the measured surface means, that the measured roughness values are introduced directly into a CAD-software where a so-called free-form surface can be generated.

Our geometrical model consists of two solid bodies with real surface topography and with layer structure, putting one on top of the other. The surfaces we have developed and used for our simulations are free-form surfaces, based on measured roughness values of a polished surface area of 1 mm^2. The density of registered points was 1 μm in both directions. The generated mathematical surface, containing all measured roughness value, is presented in *Fig. 1*/a.

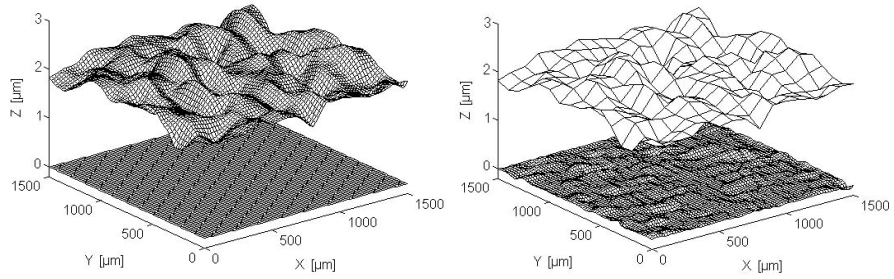

Fig. 1. The measured (1/a.) and the approximate (1/b.) surface topology

To determine the minimum needed number of grid points of the meshed surface, a comparative calculation was made between the mathematical (free-form) surface containing all measured points and another one containing a reduced number of points. This second surface was subtracted from the original one and as long as the difference-surface was near to plane, we considered that the surface which was

generated by a reduced number of points characterises satisfactorily the original one (*Fig. 1*). In this way, using the mesh resolution represented in *Fig. 2*, we could take into consideration approximately 20 roughness peaks on a surface area of 160×300 μm. The question is whether the results obtained by this surface area are generally valid for isotropic surfaces.

For the pre- and post-processing of the numerical contact model (*Fig. 2*) and to solve the numerical problem by the Finite Element Method, we used the FEA Lusas 12 software with Mystro pre- and post-processor. The mesh was generated using HX8M elements. To define the contact conditions between two solids, we used slide-surface pre-contact facility without friction.

The material of the lower solid body is C55 steel with elastic-plastic material properties, the upper one was considered as an ideal rigid body. Elastic properties are determined by Young's Modulus ($E = 2.1 \cdot 10^5$ MPa) and by Poisson's Ratio ($\nu = 0.3$). Plasticity is characterised by the flow curve of the material. Former results of FEM calculations show that the sign of the stress components changed before and after the contact of the asperities, i.e. the asperities have an alternate compression and tension stress state during the friction.

However, flow curves are generally determined under simple stress conditions, i.e. uniaxial tension or compression conditions.

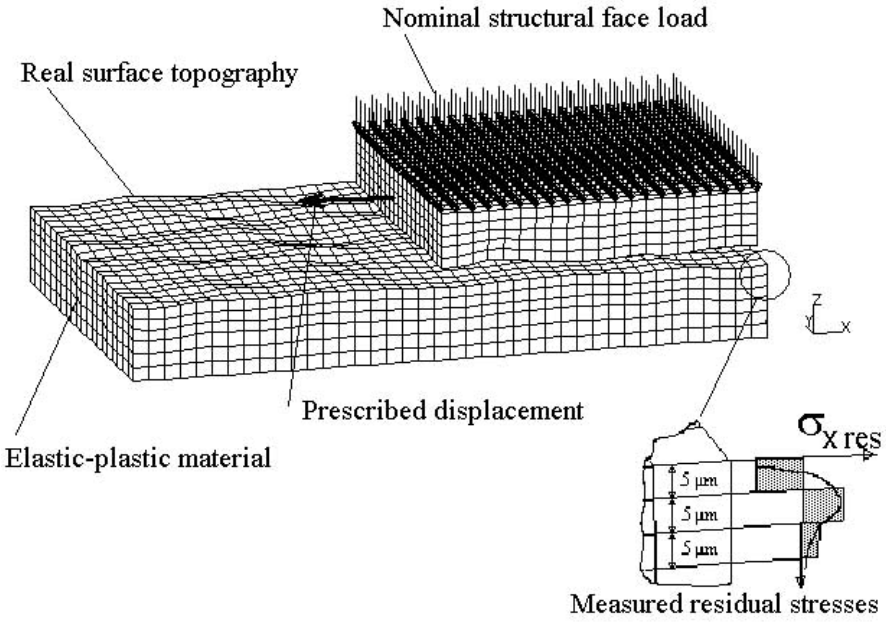

Fig. 2. The numerical contact model

To better characterise the plastic behaviour of the surface, we used the so-called cyclic flow curve (*Fig. 3*), which was put under alternate compression and

tension stress conditions. The approximate power strain hardening law of the cyclic flow curve is given by $\overline{\sigma} = 812 \cdot (\overline{\varepsilon}^{pl})^{0.15}$[MPa].

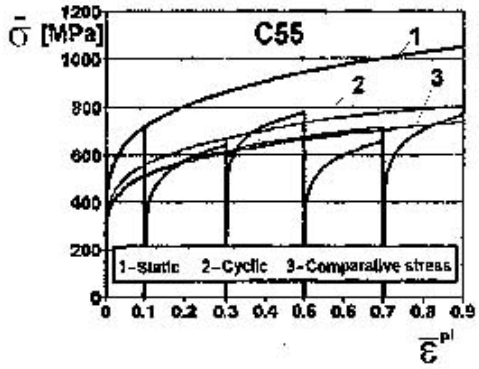

Fig. 3. The cyclic flow curve of the C55 steel [16]

The loading of the surfaces consists, on the one side, of the structural face load (50 MPa), on the other side of the rigid body-like displacement (totally 150 μm and step by step 1 μm) of the upper solid to the direction of global x axis. The elastic half-space of the lower solid was taken into consideration by elastic supports. The degree of freedom of these supports was subjected to specified spring stiffness equal to the Young's Modulus of the steels.

At the tribological processes, the existence of residual stresses developed during surface machining in the near-surface layers has a significant influence on the development of actual stress state. The residual stresses regarding their feature may be regarded as σ_x or σ_y stress component developing on the plane of the surface. If the stress state, when developing, meets the yield condition, local plastic deformation is carried out and in this way the surface layer can be locally hardened. The important influence of the steady state residual stresses on the fatigue crack initiation is explained by [17]. Following probable local plastic deformation their fraction not exceeding yield condition remains in the surface layer in measurable form and is added to the stresses developing during friction with sign. In this way, the residual compressive stresses decrease equivalent stress, in the favourable case, may only create hydrostatic compressive stress resulting in elastic deformation while the residual tensile stresses increase the brittle tendency.

In our contact model (see *Fig. 2*) the residual stress state of the polished surfaces, measured by an X-ray diffractometer, was also considered:

Surface/Depth	$0 \ldots 5$ μm	$5 \ldots 10$ μm	$10 \ldots 15$ μm
polished	$\sigma_{x\ \mathrm{res}} = -119$ MPa	$\sigma_{x\ \mathrm{res}} = -103$ MPa	$\sigma_{x\ \mathrm{res}} = 76$ MPa

To evaluate the results of the numerical analysis, we calculated the average principal strain and stress components at every nodal point, as well as the equivalent strains (in the figures: EE = Epsilon Equivalent and EPE = Epsilon Plastic Equivalent) and the equivalent stresses (SE = Sigma Equivalent). Directions of the principal strains are consistent as usual with the directions of the principal stresses and are based on the maximum value.

During the simulation, first one slide-cycle will be examined and the character of the deformation (elastic or plastic) will be observed by the evaluation of the calculated results of the numerical analysis. In the case of the elastic deformation, the nodal results will be evaluated from the point of view of fatigue of the surface (see Section 4). By the appearance of a localised plastic flow (deformation plastic), the actual deformation capacity of the given nodal points of the surface has to be considered (see Section 5) and the cycle of movement has to be repeated, on one hand, until the steady state of elastic shakedown limit is reached, on the other hand, until the exhaustion of the deformation capacity, i.e. until ductile fracture.

4. Numerical Prediction of Particle Detachment for the Case of Elastic Deformation of the Surface

If the stresses, which developed in the surface layers during one cycle of sliding, remain only elastic, then the particle detachment may be a consequence of a fatigue fracture.

Former studies traced the fatigue failure of the surface back to the fatigue of the individual roughness peaks. That was the mistake of KRAGELSKI's model [18] too. ZHARIN and co-authors [19], based on their observations through a microscope, explained the fatigue failure of the surfaces with fatigue fractures in the subsurface layers. Recent studies try to find new criteria of rupture to explain the failure under repeated cyclic stress in the case of elastic-plastic surfaces. French authors prefer to use the Dang Van criterion to predict the failure of the surface. Dang Van criterion takes into consideration separately the influence of normal and shear stress components, stressing hereby the role of the accumulation of the plastic strains due to the share stresses [8]. From the point of view of the mechanism of the failure, KAPOOR [20] and JOHNSON [21] separate the strain into two components, to a reversing (fatigue) component and to a unidirectional (ratchetting) component. The hypothesis was then made that two modes of failure can distinguish low cycle fatigue and ratchetting failure.

In the case of our numerical model, the FEM was used to predict the failure under condition of elastic stress state of the surface. The FEM offers the opportunity of giving the actual value of the damage (or the predicted lifetime) automatically in every nodal point as a function of the local equivalent stress, the loading spectrum and the fatigue-curve ($S - N$ curve) of the surface.

The fatigue behaviour of the surface layers of our model was characterised by the $S - N$ curve of the basic material (*Fig. 4*/a). To determine the loading spectrum,

we assumed that:

- during one sliding cycle the number of the theoretically possible contacts is equal to the quotient of sliding path (150 μm) and the double of the mesh parameter (2×7.5 μm),
- during one cycle all roughness peaks are loaded once by 1/3 of the total load (to have a balanced state of solid bodies, 3 contacts are needed), otherwise they are loaded proportionally to the number of the possible contacts,
- under dry friction conditions, only interrupted moving may be possible, so the total friction length is limited by 15 m which yields 10^5 cycles.

The loading spectrum is shown in *Fig. 4*/b.

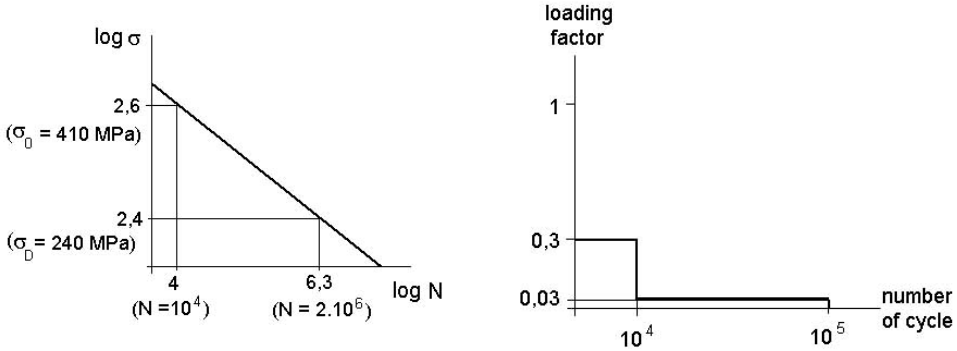

(4/a.) (4/b.)

Fig. 4. The fatigue curve of the basic material and the loading spectrum of the surface

Assuming the fatigue behaviour of the surface to be characterised by the $S-N$ curve of the basic material and using the Miner's rule, with the help of the loading spectrum, we can determine at every nodal point of the surface the total of the cumulated damage. If this value reaches one, we can assume that in this region the process of the fatigue failure may start.

In the case of the illustrated model, up to the 59th calculation step we could detect only elastic deformation in the nodal points of the surface, i.e. the equivalent stresses were smaller than the yield stress (*Fig. 5*), but at the 59th calculation step the cumulated damage exceeded the critical value (*Fig. 6*).

If the deformation state of the surface stays on the elastic field during one cycle of the moving, this simplified calculation provides the opportunity to determine the maximum admissible load as a function of the required lifetime of the surface without particle detachment.

In the case of the illustrated model, the first plastic deformation appeared at the 60th calculation step (see *Fig. 10*), so these calculated results had to be analysed in terms of ductile fracture conditions.

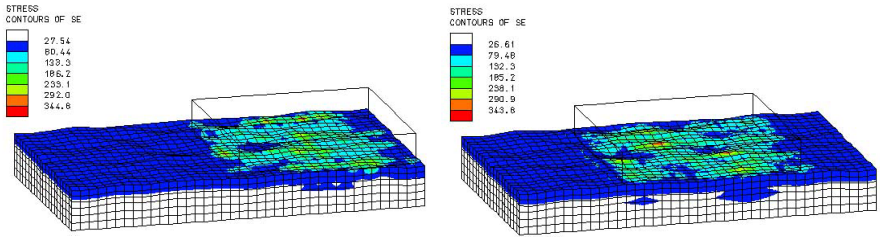

Fig. 5. Equivalent stresses (SE) in the 3rd step after the start (left) and after the beginning of the particle detachment by fatigue fracture (the values of SE are given in MPa)

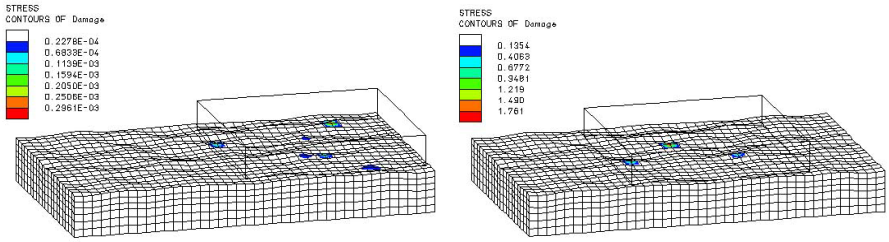

Fig. 6. The cumulated damage at the 3rd step after the start of the calculations (left) and at the beginning of particle detachment (right)

5. Numerical Prediction of Particle Detachment for the Case of Plastic Deformation of the Surface

If the plastic deformation starts at any nodal point of the surface, the mechanical process of particle detachment will be the ductile fracture. The ductile fracture will happen, if the local deformation capacity of the material exhausts for some reason. To define the conditions of particle detachment, first the deformation capacity of the given particle must be known.

Former studies, such as FLEISCHER [22], show the connection of the deformation capacity to the specific fracture work of the material. The specific fracture work (W) is a material testing index, which is equal to the work concerning a volume unit, carried out by the maximal tensile stress (σ^*), until the appearance of the ductile fracture:

$$\int_0^{\overline{\varepsilon}_f} \sigma^* \, \mathrm{d}\varepsilon = W. \tag{1}$$

In *Eq.* (1), $\overline{\varepsilon}_f$ represents the maximal strain without having a ductile fracture, i.e. the deformability or the deformation capacity of the material.

The specific fracture work can be defined by a simple tensile test, as the sum of the work of elastic deformation, the work of uniaxial (linear) plastic deformation

and the work of contraction:

$$W = W_e + W_p + W_c, \tag{2}$$

where the work of elastic deformation is:

$$W_e = \frac{\sigma_0^2}{2E}. \tag{3}$$

In this relation σ_0 is the yield stress, E is the Young's Modulus.

The work of plastic deformation to the limit of uniaxial (linear) strain (ε_m) is:

$$W_p = \frac{(\sigma_0 + 2\sigma_B)\varepsilon_m}{3}. \tag{4}$$

In this relation σ_B is the tensile strength.

The work performed during contraction is:

$$W_c = \sigma'_m \frac{\psi_c - \psi_m}{1 - \psi_m}. \tag{5}$$

In the relation σ'_m is the actual stress belonging to the maximum tensile load, Ψ_c is the contraction belonging to fracture, Ψ_m is the contraction at the end of linear strain. With the signs of *Fig. 7*:

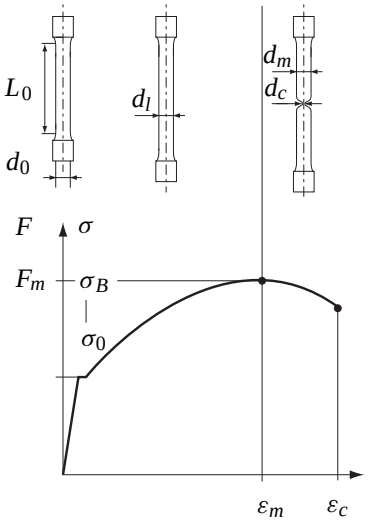

$$\sigma_m = \frac{4F_m}{d_1^2\pi}$$

$$\varepsilon_m = \frac{d_0^2 - d_m^2}{d_0^2} \tag{6}$$

$$\varepsilon_c = 1 - \frac{1}{1 + \varepsilon_c}$$

Fig. 7. Determination of the contraction work by tensile test

In our case, the specific fracture work of the examined C55 steel is 443 MJm^{-3}.

The specific fracture work in principle is an index insensitive to the structure, which changes value only if the lattice structure of the metal changes. The stresses used to define the specific deformation work and indexes of strain character, however, are sensitive to structure. They depend on the brittleness or plastic states of the material. Brittleness or plasticity are not features of the material, they only indicate their state. Therefore, brittleness or plastic state of the material depends, in addition to the structure of the material, on the state factors, i.e. on the temperature, on the speed and on the stress state. The effect of the temperature and speed could not be taken into consideration yet for the present work.

However, ZIAJA [23] verified by theoretical and experimental investigations that the specific fracture work is also dependent on the stress state. Assuming a usual plane stress state at the environment of the contact area, the dependency can be described by the following relation:

$$\int_0^{\overline{\varepsilon}_f} \sigma_1 \, \mathrm{d}\overline{\varepsilon} = \int_0^{\overline{\varepsilon}_f} \frac{\overline{\sigma}}{\sqrt{3}} \frac{2+\alpha}{\sqrt{1+\alpha+\alpha^2}} \, \mathrm{d}\overline{\varepsilon} = W. \tag{7}$$

In this relation, $\overline{\sigma}$ is the flow stress as a function of the equivalent plastic strain ($\overline{\varepsilon}^{pl}$) and α is a factor describing the deformation history. The interpretation range of α is in this case:

$$-1/2 < \alpha = \mathrm{d}\varepsilon_2/\mathrm{d}\varepsilon_1 < 1. \tag{8}$$

For the case of the strain hardening power law, the flow stress is defined as $\overline{\sigma} = K \cdot (\overline{\varepsilon}^{pl})^n$, the integration can be carried out in closed form, and the deformation capacity ($\overline{\varepsilon}_f$) as a function of the actual stress state can be defined as:

$$\overline{\varepsilon}_f = \left[\frac{W(1+n)}{K} \frac{\sqrt{3(1+\alpha+\alpha^2)}}{2+\alpha} \right]^{\frac{1}{1+n}}. \tag{9}$$

In the case of our material, the value of the deformation capacity can vary between 0.59 and 0.67 in the given interpretation range.

To characterise the deformation state of the particles of the surface depending on the actual local stress state, a reserve of plasticity (RP) was calculated at every nodal point:

$$RP = 1 - \frac{EPE}{\overline{\varepsilon}_f}. \tag{10}$$

Calculating the value of $\alpha = \mathrm{d}\varepsilon_2/\mathrm{d}\varepsilon_1 \cong \varepsilon_2^{pl}/\varepsilon_1^{pl}$ continuously during the numerical analysis and using *Eq.* (9), it is possible to determine the deformation capacity step by step at every nodal point. If this reserve of plasticity exhausts, i.e. the equivalent plastic strain (EPE) attains the deformation capacity ($\overline{\varepsilon}_f$), the reserve of plasticity will be zero at the given nodal point and the particle detachment, as a result of a ductile fracture, may happen.

The calculated results were drawn in two positions in both models just before the critical deformation state and one step after it:

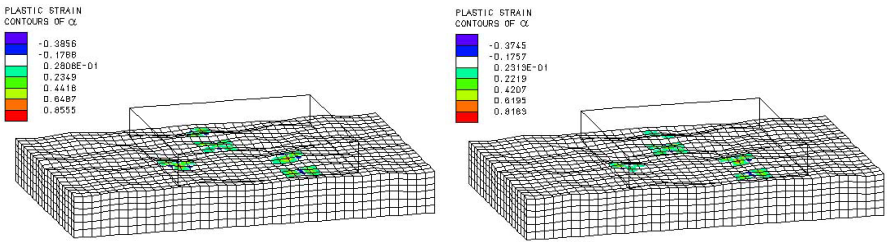

Fig. 8. The variation of α before (left) and after (right) the critical deformation state

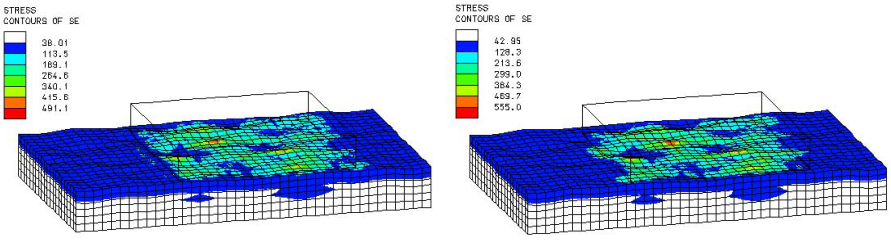

Fig. 9. Equivalent stresses before (left) and after (right) the critical state causing the particle detachment

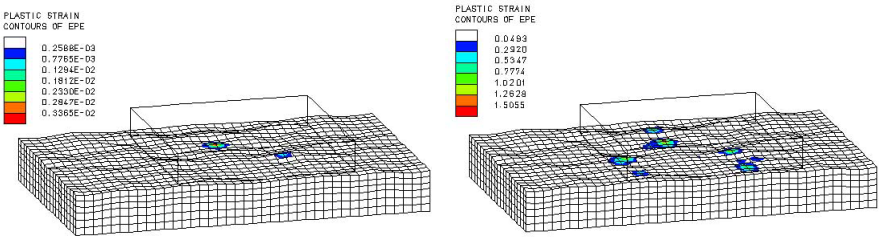

Fig. 10. Equivalent plastic strains (EPE) before (left) and after (right) the critical deformation state

6. Results and Conclusions

Today's computing techniques allow to analyse the three-dimensional contact problems with the help of the Finite Element Method. This paper presented a numerical simulation technique for calculating the strain and the stress state during one or more sliding cycles at every nodal point of the surfaces containing real roughness topology and layered structure. Depending on the nature of deformation, one can evaluate the actual stress and strain state either from the point of view of the fatigue failure or from the point of view of the exhaustion of deformation capacity of the surfaces.

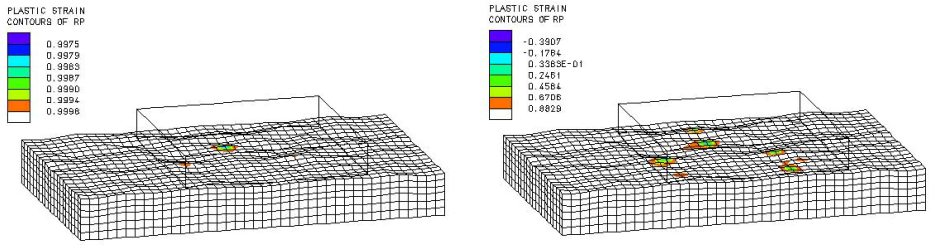

Fig. 11. The values of the reserve of plasticity (RP) before (left) and after (right) the beginning of the particle detachment by ductile fracture

The presented calculation results show that the contact remains elastic until the real contact area is sufficiently large to distribute the contact pressure. Differently from this, the plastic deformation of the roughness peaks begins and – based on the presented results – the plastic strain, considering the strain hardening process, exceeds the deformation capacity of the base material even in the case of the first plastic contact. Using the flow power strain hardening law of the basic material and limiting the maximum plastic strain by the deformation capacity, which was calculated from the specific fracture work, it was not possible to demonstrate plastic ratchetting. To simulate the ratchetting mechanism, it is necessary to ensure that the surface be able to tolerate large plastic strains to fracture, i.e. one has to define perfectly-plastic properties compared to the substrate for the surface layer. The perfect plasticity may be a consequence of the high hydrostatic component of stress or of the superimposed hydrostatic pressure in concentrated contacts, but this phenomenon could not be verified by the presented model under dry friction conditions.

Our numerical model is not able yet to simulate quantitatively the wear, but it is possible to predict the probable degradation mechanism of the surfaces considering their nominal load and the required lifetime. Through this methodology, it would be possible to optimize the manufacturing of the surfaces or the use of antiwear coatings in the future.

Acknowledgement

We are grateful to Prof. J.A. Williams from the University of Cambridge for reviewing our manuscript and for his remarks.

This work was supported by the Hungarian Scientific Research Fund (OTKA) under project No. T 016007.

Nomenclature

$\sigma_{x\ \mathrm{res}}$ – residual (initial) stress
E – Young's Modulus
ν – Poisson's Ratio
$\overline{\sigma}$ – flow stress
$\overline{\varepsilon}^{pl}$ – equivalent plastic strain
σ_0 – yield stress
σ_D – fatigue limit
σ^* – maximal tensile stress
$\overline{\varepsilon}_f$ – deformation capacity
W – specific fracture work
W_e – work of elastic deformation
W_p – work of plastic deformation
W_c – work of contraction
ε_m – limit of uniaxial (linear) strain
σ_B – tensile strength
σ'_m – actual stress at maximal tensile load
Ψ_c – contraction at fracture
Ψ_m – contraction at the end of the linear strain
σ_m – actual (true) stress at the end of the uniaxial strain
F_m – maximum load
d_0 – initial diameter of the tensile specimen
d_1 – diameter of the tensile specimen at the end of the uniaxial strain
d_m – diameter of the cylindrical part of the tensile specimen at fracture
ε_c – contraction strain
α – factor describing the deformation history ($= \mathrm{d}\varepsilon_2/\mathrm{d}\varepsilon_1$)
K – constant of the flow power strain hardening law
n – exponent of the flow power strain hardening law
RP – reserve of plasticity

References

[1] GODET, M.: Third-Bodies in Tribology, *Wear*, **136** (1990), pp. 29–45.
[2] BERTHIER, Y.: The Third Body Concept: Interpretation of Tribological Phenomena, *Tribology Series, 31, Proceedings of the 22nd Leeds-Lyon Symposium on Tribology*, Elsevier, (1996), pp. 21–29.
[3] SEMENYUK, N. F. – BACHINSKAYA, N. K.: Analytical Model of Rough Surfaces Contact, *Journal of Friction and Wear*, **14**, No. 5, (1993), pp. 24–28.
[4] KOPALINSKY, E. M. – OXLEY, P. L. B.: Explaining the Mechanics of Metallic Sliding Friction and Wear in Terms of Slipline Field Models of Asperity Deformation, *Wear*, **190** (2), (1996), pp. 145–154.
[5] TORRANCE, A. A. – BUCKLEY, T. R.: A Slip-line Model of Abrasive Wear, *Wear*, **196** (1–2), (1996), pp. 35–45.

[6] KAPOOR, A. – JOHNSON, K. L. – WILLIAMS, J. A.: A Model for the Mild Ratchetting Wear of Metals, *Wear*, **200** (1996), pp. 38–44.
[7] VÁRADI, K. – NÉDER, Z. – FRIEDRICH, K.: Evaluation of the Real Contact Areas, Pressure Distributions and Contact Temperatures During Sliding Contact Between Real Metal Surfaces, *Wear*, **200** (1–2), (1996), pp. 55–62.
[8] STALIN-MULLER, N. – DANG VAN, K.: Numerical Simulation of the Sliding Wear Test in Relation to Material Properties, *Wear*, **203–204** (1–2), pp. 180–186.
[9] NOGI, T. – KATO, T.: Influence of a Hard Surface Layer on the Limit of Elastic Contact – Part I: Analysis Using a Real Surface Model, *Journal of Tribology*, **119** (1997), pp. 493–500.
[10] XIE, Y. – WILLIAMS, J. A.: The Generation of Worn Surfaces by Repeated Interaction of Parallel Grooves, *Wear*, **162–164** (1993), pp. 864–872.
[11] CHIZHIK, S. A. – GORBUNOV, V. V. – MYSKHIN, N. K.: Computer Modelling of the Solids Contact Zone Based on the Scanning Probe Microscopy, *Journal of Friction and Wear*, **14**, No. 4, (1993), pp. 5–12.
[12] ANDO, Y. – INO, J.: The Effect of Asperity Array Geometry on Friction and Pull-Off Force, *Journal of Tribology*, **119** (1997), pp. 781–785.
[13] LUNDE, L. – TONDER, K.: Numerical Simulation of the Effects of Three-Dimensional Roughness of Hydrodynamic Lubrication: Correlation Coefficients. *Journal of Tribology*, **119** (1997), pp. 315–317.
[14] LUNDE, L. – TONDER, K.: Pressure and Shear Flow in a Rough Hydrodynamic Bearing, Flow Factor Calculation. *Journal of Tribology*, **119** (1997), pp. 549–555.
[15] AI, X.: Effect of Three-Dimensional Random Surface Roughness on Fatigue Life of a Lubricated Contact, *Journal of Tribology*, **120** (1998), pp. 159–164.
[16] SZABADÍTS, Ö., – KRÁLICS, GY. – LOVAS, J.: Bestimmung zyklischer Fließkurven zur Berechnung von Blechumformvorgängen, *Blech Rohre Profile* **41**, 3 (1994), pp. 190–194.
[17] YU, C. C. – KEER, L. M. – STEELE, R. K.: Three-Dimensional Residual Stress Effects on the Fatigue Crack Initiation in Rails, *Journal of Tribology*, **119** (1997), pp. 660–666.
[18] KRAGELSKI, I. V.: Reibung und Verschleiß, VEB Verlag Technik, Berlin, 1971.
[19] ZHARIN, A. L. – SHIPITSA, N. A. – FISHBEIN, E. I.: Some Features of Fatigue at Sliding Friction, *Journal of Friction and Wear*, **14**, No. 4 (1993), pp. 13–22.
[20] KAPOOR, A.: A Re-evaluation of the Life to Rupture of Ductile Metals by Cyclic Plastic Strain, 1994, *Fatigue Fract. Engng. Mater. Struct.* **17**, No. 2, pp. 201–219.
[21] JOHNSON, K. L.: Contact Mechanics and the Wear of Metals, *Wear* **190** (1995), pp. 162–170.
[22] FLEISCHER, G. – GRÖGER, H. – THUM, H.: Verschleiß und Zuverlässigkeit, VEB Verlag Technik, Berlin, 1980, pp. 124.
[23] ZIAJA, GY. – CSER, L. – DARVAS, Z.: Simulation and Limit State in Metal Forming, Advanced Technology of Plasticity, *Proceedings of the Second Conference on Technology of Plasticity*, Ed. Lange, K., Springer Verlag, Berlin etc., Vol.II., (1987), pp. 999–1003.